Postseismic deformation of the Andaman Islands following the 26 December, 2004 Great Sumatra–Andaman earthquake

J. Paul,[1] A. R. Lowry,[2] R. Bilham,[3] S. Sen,[4] and R. Smalley Jr.[1]

Received 20 June 2007; revised 20 August 2007; accepted 5 September 2007; published 13 October 2007.

[1] Two years after the Great Sumatra-Andaman earthquake the 3.1 m WSW coseismic displacement at Port Blair, Andaman Islands, had increased by 32 cm. Postseismic uplift initially exceeded 1 cm per week and decreased to <1 mm/week. By 2007 points near Port Blair had risen more than 20 cm, a 24% reversal of coseismic subsidence. Uplift at eight GPS sites suggests a gradual eastward shift of the coseismic neutral axis separating subsidence from uplift. Simulations of the GPS postseismic displacements as viscoelastic relaxation of coseismic stress change and as slip on the plate interface indicate that slip down-dip of the seismic rupture dominates near-field deformation during the first two years. Postseismic slip beneath the Andaman Islands released moment equivalent to a magnitude $M_w \geq 7.5$ earthquake, and the distribution suggests deep slip in the stable frictional regime accelerated to catch up to the coseismic rupture. **Citation:** Paul, J., A. R. Lowry, R. Bilham, S. Sen, and R. Smalley Jr. (2007), Postseismic deformation of the Andaman Islands following the 26 December, 2004 Great Sumatra–Andaman earthquake, *Geophys. Res. Lett.*, *34*, L19309, doi:10.1029/2007GL031024.

1. Introduction

[2] The December 26th 2004, M_w = 9.3 Sumatra-Andaman earthquake ruptured 1600 km of subduction thrust at the east boundary of the Indian plate. In addition to several meters of southwestward coseismic displacement (Figure 1, inset), Global Positioning System (GPS) instruments measured 60 cm of coseismic uplift at Diglipur in the Northern Andaman Islands, 84 cm subsidence at Port Blair, 7 cm subsidence at Havelock island, and 34 cm uplift at Hut Bay [*Freymueller et al.*, 2007]. Remote sensing and visual inspection of shoreline changes provide evidence for both uplift and subsidence, ranging from +40 to −70 cm, which *Meltzner et al.* [2006] characterize as separated by a hinge line. Others have used the term pivot line. Because the coseismic surface flexure is not truly a planar tilt, in this article we refer to this line of zero uplift as a neutral axis. Postseismic processes discussed here have translated this line eastward (Figure 1).

[3] We collected GPS measurements of postseismic deformation at eleven sites in the Andaman Islands (Figures 1 and 2). We initiated continuous GPS recording at Port Blair (CARI) three weeks after the earthquake, Havelock (HAV2) in January 2007, and on Little Andaman (HUTB) in December 2006. Other sites were occupied for periods of several days at intervals of several months. The data afford sufficient spatial and temporal sampling to characterize near-field postseismic deformation.

[4] Three deformation processes are likely candidates for postseismic response to coseismic stress change: (1) poroelastic relaxation moderated by flow of interstitial fluids [*Peltzer et al.*, 1998]; (2) viscoelastic relaxation of the mantle [*Rundle*, 1978]; and (3) aseismic slip in velocity-strengthening frictional conditions [*Tse and Rice*, 1986]. Surface deformation caused by these processes can look similar, such that the effects of one process may be mismodeled using the physics of another [*Thatcher and Rundle*, 1979; *Fialko*, 2004]. Laboratory deformation experiments leave little doubt that all three processes contribute to transient deformation after earthquakes, but the relative contribution of each should depend on temporal and spatial scales of measurement. Where data are adequately sampled in both time and space, all three processes may be required to fit the observations [*Freed et al.*, 2006]. However examples of great earthquake postseismic deformation sampled densely in both time and space are few. Consequently questions remain as to the roles of these three processes in the earthquake cycle, and even whether they play a similar role on all fault zones or in subsequent events on the same fault zone.

[5] In this article we combine campaign and continuous GPS data to examine end-member models of postseismic deformation. The first two years of near-field Andaman deformation predominantly reflects postseismic slip down-dip of the coseismic rupture, consistent with simulations of frictional slip dynamics.

2. Data and Analysis

[6] GPS measurements were initiated at six sites (CARI, WNDR, HAVE, RUTL, RMNG and MHRT) within two to six weeks after the earthquake. We collected three to five epochs of data at seven sites during the first two years (Figure 2). All of the campaign GPS monuments consist of steel pins drilled into rock. At continuous sites, monuments consist of 4 m concrete pillars that rise to 2 m above ground. At 2 m depth, the pillars are anchored to a 30 cm thick, 4 × 4 m reinforced concrete foundation. Data analysis at the University of Memphis used GAMIT/GLOBK. Twelve regional IGS sites were used to determine the ITRF2000 reference frame.

[7] In the first two years beginning 20 days after the mainshock, station CARI moved 7.5 cm south, 31 cm west

[1]Centre for Earthquake Research and Information, Memphis, Tennessee, USA.
[2]Department of Geology, Utah State University, Logan, Utah, USA.
[3]Department of Geological Sciences, University of Colorado, Boulder, Colorado, USA.
[4]Society for Andaman and Nicobar Ecology, Middle Point, Port Blair, India.

0094-8276/07/2007GL031024$05.00

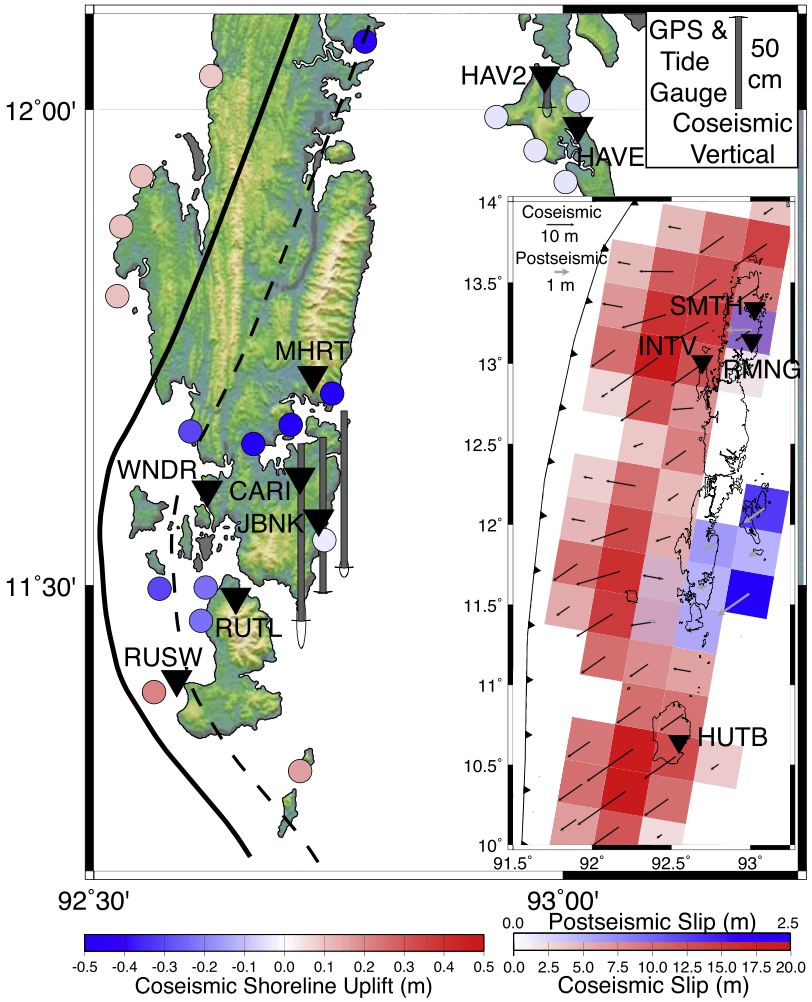

Figure 1. Andaman Islands uplift. Black inverted triangles are GPS sites measured for postseismic displacement in this study. Circles are remote-sensed coseismic shoreline uplift from *Meltzner et al.* [2006]; solid line is their estimate of neutral axis separating western uplift from eastern subsidence. Gray vectors are coseismic vertical from GPS and tide gauge. Dashed line approximates current neutral axis summing coseismic and postseismic. Inset shows best-fit models of Andaman coseismic fault slip from GPS data summarized by *Freymueller et al.* [2007] (red with black vectors), and postseismic slip from GPS data described here (blue with gray vectors).

and rose ~23 cm (Figure 2). All of the campaign sites exhibit uplift and SW to WSW motion, but magnitudes vary by up to 20% and azimuths differ by as much as 36°. Motion at Mount Hariot (MHRT) and Rangachang (JBNK) is very similar to that at nearby CARI. Wandoor (WNDR) and Rutland (RUTL) have smaller, more westerly displacements than sites further east. HAVE and continuous site HAV2 both exhibit a large southward component of motion. Ramnagar (RMNG) moved the least among the well-sampled sites.

[8] Prior to the earthquake, four epochs of campaign GPS measurement were collected at a site near CARI in 1996–1999 (CARO, subsequently destroyed). Our reanalysis of CARO data indicates 9.3 ± 1.8 mm/yr right-lateral oblique convergence with the Indian plate [*Paul et al.*, 2001]. How this relates to India–Burma relative plate motion depends on unknown coupling of the two, and the true plate convergence rate is probably more than twice this [e.g., *Socquet et al.*, 2006]. The Andamans are approximately 100 km from the trench, and GPS measurements of coseismic rupture suggest that Port Blair lies slightly east of the downdip terminus (Figure 1, inset).

3. Modeling

3.1. Exponential Fit of GPS Time Series

[9] To compare the mix of continuous and campaign data with model predictions, we first estimate transient displacements at each site. CARI is the best-sampled GPS site (Figure 2), and the coordinate time series $\vec{x}(t)$ there suggests an exponential decay of the form

$$\vec{x}(t) = \vec{x}_0 + \vec{V}t - \vec{A}_0\left[1 - \exp\left(\frac{T_0 - t}{\tau}\right)\right] \quad (1)$$

in which $\vec{V}$ is constant (interseismic) velocity, T_0 is time of the Great Sumatra/Andaman earthquake, τ is characteristic timescale of the decay, and $\vec{A}_0$ is transient displacement in the limit as $t \rightarrow \infty$.

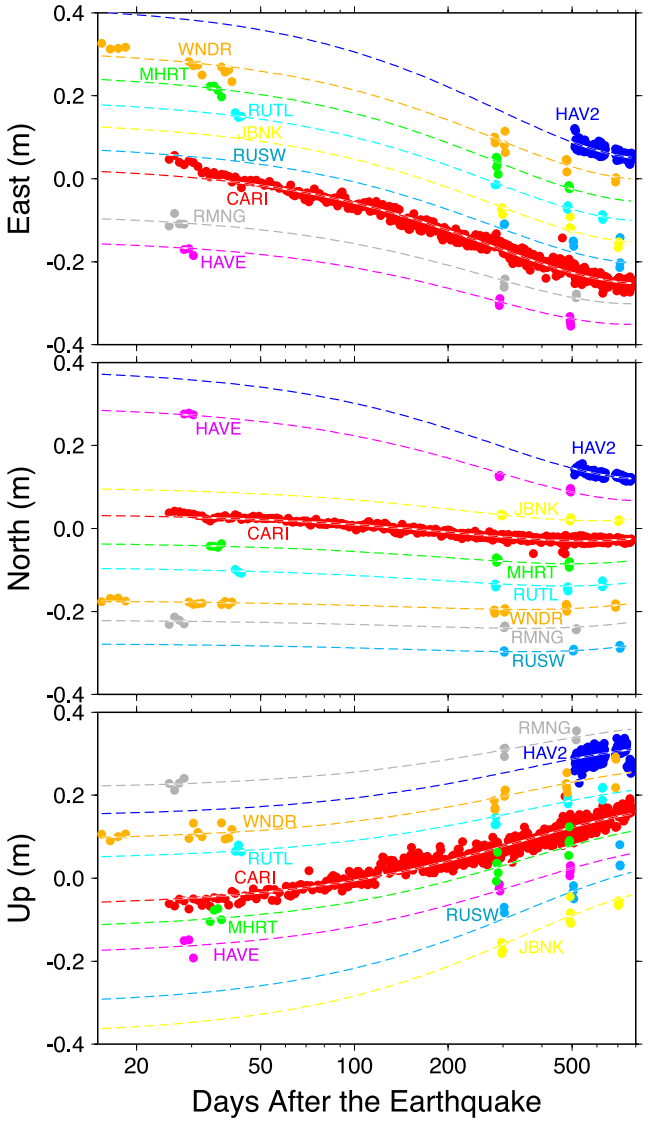

Figure 2. Daily coordinate solutions at Andaman GPS sites versus log-scaled time after the earthquake. Dashed lines are best-fit models of exponential decay plus interseismic velocity.

[10] Interseismic velocity is assumed to be $\vec{V}$ = (3.59, 3.02, 0.00) cm/yr at all of the sites, i.e., velocity at CARO in the ITRF-2000 frame of the postseismic data. This assumption will be correct (within uncertainties) at nearby CARI, but interseismic slip modeling in other subduction zones [e.g., *Lowry*, 2006] suggests this introduces errors of up to 5 mm/yr at the other sites (i.e., <3% of the ~35–50 cm transient displacements). Displacement terms $\vec{A}_0$ are estimated by weighted least-squares fit of the data to equation (1). The choice of τ minimizing the weighted L_2-norm misfit is determined by grid search. Simultaneous parameter inversion of all the Andaman GPS time series yields an exponential decay timescale τ = 0.82 + 0.07/−0.06 years at 95% confidence. Estimates of horizontal and vertical transient displacement are depicted in Figure 3. Here we show displacements estimated for the period T_0–2007.0 (i.e., we multiply $\vec{A}_0$ by 0.914 to represent partially completed decay).

3.2. Viscoelastic Relaxation

[11] We used VISCO1D [*Pollitz*, 1997] to model viscoelastic response of a self-gravitating, layered spherical earth. Sumatra/Andaman coseismic slip was approximated as three fault planes dipping 15° to 40 km depth. Coseismic slip was approximated from seismic and geodetic estimates [e.g., *Lay et al.*, 2005; *Freymueller et al.*, 2007] including 7 m of slip on the northernmost (Andaman) segment. We modeled the viscoelastic response for Earth models with a 40–80 km range of thicknesses for the elastic lithosphere, upper mantle (<670 km depth) Maxwell viscosity of η_{UM} = 5×10^{16}–10^{21} Pa s, and lower mantle viscosity 10^{21} Pa s.

[12] Figure 3 compares the GPS observations to the best-fitting Earth model, which assumed a 70 km elastic layer over a 5×10^{17} Pa s upper mantle viscosity. Total displacements for the 2004.98–2007.0 epochs fit the GPS observations within uncertainties at some sites (e.g., HAV2), but predicted displacements change by <4 cm across the Andaman network aperture. The GPS observations by contrast exhibit large displacement gradients. Modeled displacement directions and gradients are insensitive to assumed upper mantle viscosity, but magnitude is very sensitive, and lower viscosities yield correspondingly larger motions. Even where modeled and observed displacement vectors are similar, however, the time dependence of displacement is not. The decay time for the best-fitting $\eta_{UM} = 5 \times 10^{17}$ Pa s model is 2.7 + 0.8/−0.5 years at 95% confidence, after fitting an exponential to the first two years of modeled displacement at CARI (Figure 3, inset a). This differs from the τ = 0.82 year timescale of the GPS data at ≫99% confidence. Introducing a factor-of-3.3 lower viscosity to match the model decay timescale to the GPS observations would increase correspondingly the displacement vector magnitudes.

3.3. Postseismic Slip

[13] To compare the data to a postseismic slip end-member, we modified slip modeling software developed for slow slip events in southern Mexico [*Lowry*, 2006]. GPS positions $\vec{x}(t)$ were modeled as

$$\vec{x}(t) = \vec{x}_0 + \vec{V}t + \oint \vec{S}\left(\vec{\zeta}, t\right) G\left(\vec{x}, \vec{\zeta}\right) \mathrm{d}\vec{\zeta}. \tag{2}$$

Here, $\vec{\zeta}$ denotes location on the fault surface, G is the deformation Green's function [*Okada*, 1985], and $\vec{S}$ describes the transient slip. Ideally $\vec{S}$ would be parameterized using frictional constitutive laws, but as a first approximation we let

$$\vec{S}\left(\vec{\zeta}, t\right) = -\vec{S}_0\left(\vec{\zeta}\right) \exp\left(\frac{T_0 - t}{\tau}\right) \tag{3}$$

in which $\vec{S}_0$ is the total transient slip anticipated following the earthquake.

[14] We used the transient displacements $\vec{A}_0^i$ estimated at each of the GPS sites i to invert for anomalous slip $\vec{S}_0$ on a 30 km mesh representation of a fault surface approximated from aftershocks and other well-located earthquakes on the plate interface. We inverted for both strike-slip and dip-slip. To regularize the solution, we required strike-slip not to exceed dip-slip and imposed a minimization of the total

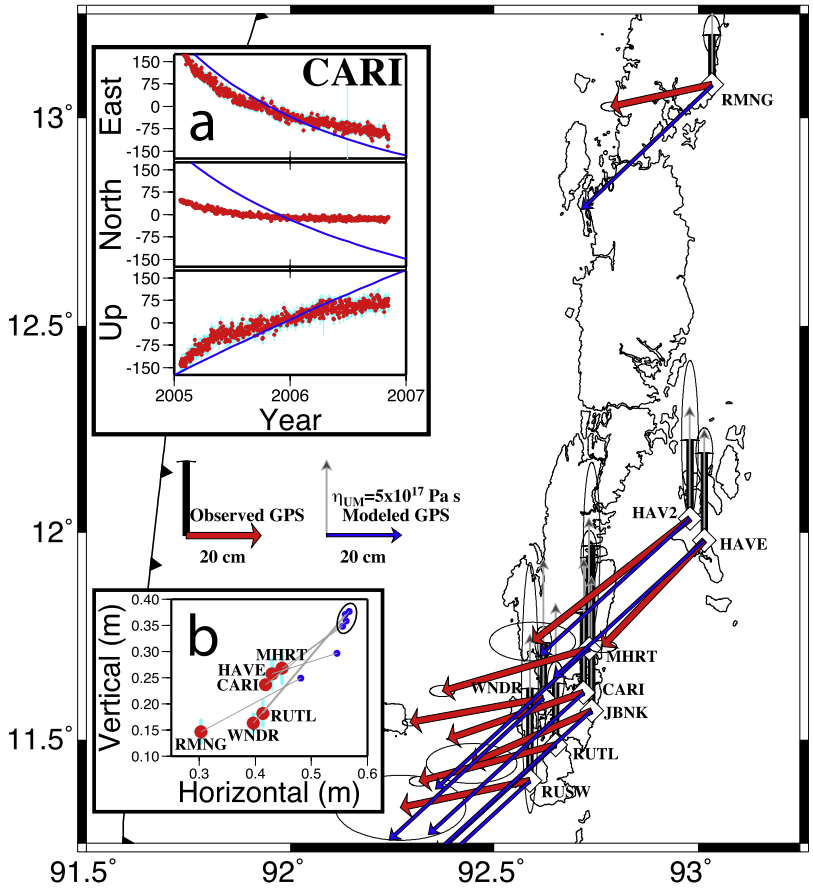

Figure 3. GPS-observed and viscoelastic-modeled postseismic displacements. Red vectors/black bars are 2004.98–2007.0 horizontal/vertical displacements, respectively, from exponential fit of the GPS data, with scaled 95% confidence ellipses. Best-fit model of viscoelastic relaxation is depicted as blue/dark grey vectors. Inset a shows comparison of CARI GPS coordinates (red circles) to best-fit model (blue line). Inset b shows vertical versus horizontal transient displacement; red is GPS estimate (with 2σ error), blue is viscoelastic model. Predictions for South Andaman sites are circled.

moment release. The latter constraint penalizes slip far from the GPS data constraint. The best-fit model of slip on the subduction interface is depicted in Figure 4.

4. Discussion and Conclusions

4.1. Relative Importance of Relaxation Processes

[15] Despite similarities, models of the three relaxation processes do differ. Viscoelastic models poorly match the directions, magnitudes, displacement gradients, and time-dependence of the GPS measurements. A better fit to the observations might be obtained by further varying fault dislocation and viscosity parameterizations, but a fit as good as the fault slip model is unlikely to be physically viable. To match the timescale parameter $\tau = 0.82$ years estimated for exponential decay would require a uniform Maxwell viscosity $\eta \sim 7 \times 10^{16}$ Pa s. Such a low viscosity is conceivable if the mantle is extremely water-rich and strain rate $\dot{\epsilon}$ exceeds background rates by several orders of magnitude, given that $\eta \propto \dot{\epsilon}^{\frac{1-n}{n}}$ for power-law creep. Matching other observations to a viscoelastic model would stretch limits of credibility even further. For example, sites MHRT, CARI, WNDR and RUTL on South Andaman are spaced only 10–25 km apart, but their vertical displacements vary by up to 40%. The spatial wavelength of vertical response to a deformation point source is roughly equal to the depth, so large variations can be modeled as fault slip at the 35–40 km depth of the plate interface (Figure 4). Spatial wavelengths of viscoelastic response are filtered twice however: once to propagate stress from the dislocation to the depth of ductile creep, and again thence to the surface. The temperature structure for subduction of ~100 Myr-old oceanic lithosphere would preclude creep above ~80 km depth in this region, and the 70 km elastic lithosphere assumed in our best-fit model predicts only 7% variation in the vertical response of South Andaman sites (circled in Figure 3, inset b). These observations lead us to conclude viscoelastic relaxation does not dominate the first two years of Andaman near-field deformation.

[16] The strongest evidence against poroelasticity derives from displacement directions. Models of postseismic fluid diffusion [e.g., *Fialko*, 2004] predict maximum uplift over loci of positive coseismic dilatational strain, and subsidence over contractional strain. Horizontal motions are away from the uplift and toward subsidence, vanishing where vertical displacements are largest and maximal between a fluid source and sink where vertical displacement is ~0. Hence, on a plot of vertical versus horizontal displacement, the distribution of measurements should have negative slope.

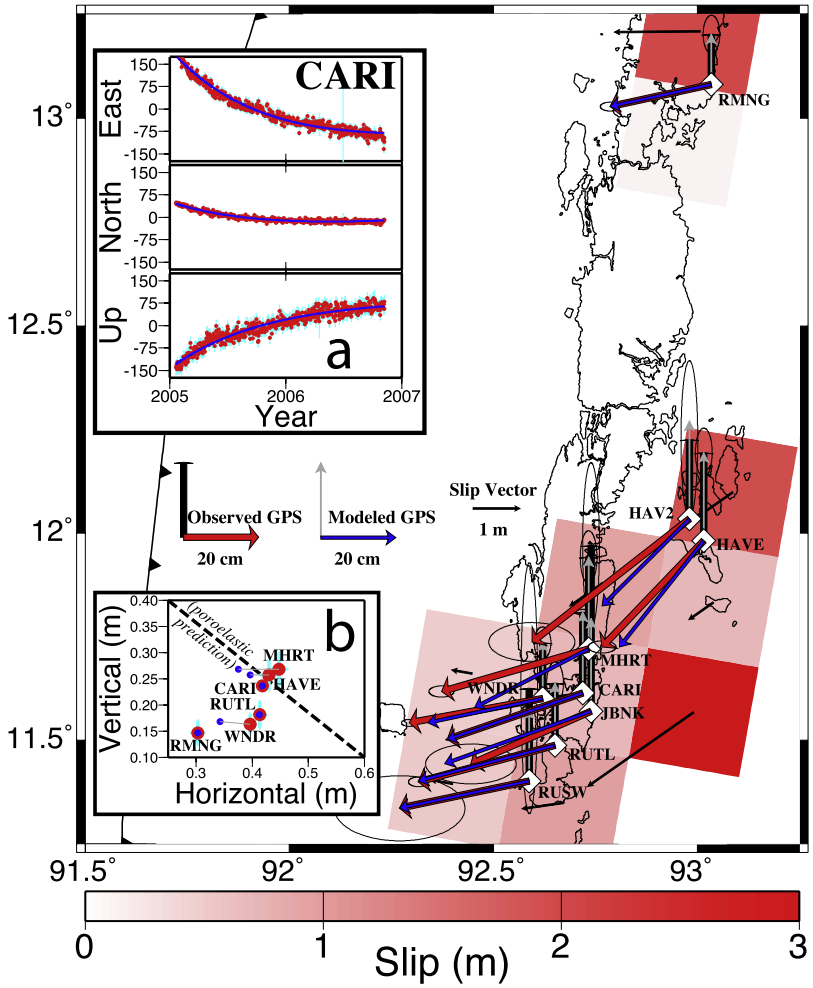

Figure 4. Andaman data modeled as slip on the subduction thrust. Red vectors are 2004.98–2007.0 displacements from exponential fit of the GPS data, with scaled 95% confidence ellipses. Blue vectors are the best-fit model of postseismic slip. Red patches with thin black vectors indicate the magnitude and direction of modeled slip. Inset a shows comparison of CARI GPS coordinates (red circles) to best-fit model (blue line). Inset b shows vertical versus horizontal transient displacement; red is GPS estimate (with 2σ error), blue is slip model. Dashed line schematically shows negative slope of poroelastic response.

Inset b of Figures 3 and 4 exhibits a positive slope distribution.

[17] Although fault slip apparently dominates the Andaman Islands postseismic response, both viscoelastic and poroelastic processes must contribute. Viscoelastic modeling using reasonable viscosity structures predict displacements of up to 8 cm during the 2004.98–2007.0 epoch. Models of poroelastic response to earthquakes elsewhere also predict displacements of order several cm [e.g., *Fialko*, 2004]. Hence, one reasonably might expect up to 25% error modeling the deformation as pure fault slip. Inspection of residuals at IGS sites used in our analysis suggest an additional $\leq$3% error in realization of the reference frame, related to large-scale postseismic deformation. Separating these effects will require additional data that sample the differing temporal and spatial scales of the three processes, and future efforts will address this.

4.2. Implications of the Slip Model

[18] We modeled ten coseismic GPS vectors summarized by *Freymueller et al.* [2007] using a minimum-moment constraint. The best-fit estimate of slip averaged 9.8 m within a rupture zone averaging about 90 km width (Figure 1, inset). The corresponding coseismic moment release for the 500 km Andaman segment is equivalent $M_w = 8.6$, comparable to the *Freymueller et al.* [2007] $M_w = 8.5$ estimate in five rectangular dislocation patches, and also consistent with the $M_w = 8.6$ estimate from seismic data after combining the rapid (1–2 m in the first ten minutes) and slow (5 m over the next hour) slip averaged over a 160 km width [*Lay et al.*, 2005].

[19] Despite possible contamination by other processes, the postseismic slip model is intriguing. The minimum-moment constraint images slip only where data are available, but there the slip magnitude and relative contribution of strike slip increase with depth. Slip vectors at depth mirror the surface GPS displacements, which are smaller and more trench-normal at western sites (Figure 4). Postseismic moment release is equivalent to a $M_w \geq 7.5$ earthquake, or about 10% of coseismic, and is probably

larger given that a small fraction of the Andaman segment is sampled by data presented here.

[20] Postseismic slip overlaps slightly with the coseismic slip estimate (Figure 1, inset), but most of the moment release is further downdip. This pattern mirrors simulations of coseismic and postseismic slip in elastodynamic models of rate- and state-dependent friction [e.g., *Lapusta et al.*, 2000], in which slip deficit accumulates in velocity-strengthening conditions during interseismic periods and catches up to coseismic slip over several years' time. Andaman data prior to 2004 are insufficient to assess interseismic coupling where we now identify postseismic slip. However modeling of interseismic slip and stress rates from GPS data at the Cocos-North America subduction boundary suggests locking above the frictional transition buffers stress accumulation in the shallow velocity-strengthening regime [*Lowry*, 2006], thus enabling slip deficit to accumulate that can drive slip following an earthquake.

[21] **Acknowledgments.** We thank V. K. Gaur (Indian Institute of Astrophysics), Samir Acharya (Society of Andaman and Nicobar Ecology) and T. V. R. S. Sharma (Central Agricultural Research Institute) for their partnership in this project. We also thank Anjan Battacharya for obtaining permission to set up GPS site CARI, and Tom Herring for help and advice on GAMIT processing. This paper was improved by thoughtful suggestions of reviewers Cristophe Vigny and Fred Pollitz. CERI publication 517. Support for this research was provided by NSF grants EAR-0523319 and EAR-0537559.

References

Fialko, Y. (2004), Evidence of fluid-filled upper crust from observations of postseismic deformation due to the 1992 M_w7.3 Landers earthquake, *J. Geophys. Res.*, *109*, B08401, doi:10.1029/2004JB002985.

Freed, A. M., R. Brgmann, E. Calais, J. Freymueller, and S. Hreinsdttir (2006), Implications of deformation following the 2002 Denali, Alaska, earthquake for postseismic relaxation processes and lithospheric rheology, *J. Geophys. Res.*, *111*, B01401, doi:10.1029/2005JB003894.

Freymueller, J. T., A. Shuler, C. P. Rajendran, A. Earnest, and K. Rajendran (2007), Coseismic and preseismic displacements in the Andaman and Nicobar islands, and implications for the regional tectonics, *Bull. Seismol. Soc. Am.*, in press.

Lapusta, N., J. R. Rice, Y. Ben-Zion, and G. Zheng (2000), Elastodynamic analysis for slow tectonic loading with spontaneous rupture episodes on faults with rate- and state-dependent friction, *J. Geophys. Res.*, *105*, 23,765–23,789.

Lay, T., et al. (2005), The great Sumatra-Andaman earthquake of 26 December 2004, *Science*, *308*(5725), 1127–1133.

Lowry, A. R. (2006), Resonant slow fault slip in subduction zones forced by climatic load stress, *Nature*, *442*(7104), 802–805.

Meltzner, A. J., K. Sieh, M. Abrams, D. C. Agnew, K. W. Hudnut, J.-P. Avouac, and D. H. Natawidjaja (2006), Uplift and subsidence associated with the great Aceh-Andaman earthquake of 2004, *J. Geophys. Res.*, *111*, B02407, doi:10.1029/2005JB003891.

Okada, Y. (1985), Surface deformation due to shear and tensile faults in a half-space, *Bull. Seismol. Soc. Am.*, *75*, 1135–1154.

Paul, J., et al. (2001), The motion and active deformation of India, *Geophys. Res. Lett.*, *28*(4), 647–650.

Peltzer, G., P. Rosen, F. Rogez, and K. Hudnut (1998), Poroelastic rebound along the Landers 1992 earthquake surface rupture, *J. Geophys. Res.*, *103*, 30,131–30,145.

Pollitz, F. F. (1997), Gravitational-viscoelastic postseismic relaxation on a layered spherical Earth, *J. Geophys. Res.*, *102*, 17,921–17,941.

Rundle, J. B. (1978), Viscoelastic crustal deformation by finite, quasi-static sources, *J. Geophys. Res.*, *83*, 5937–5945.

Socquet, A., C. Vigny, N. Chamot-Rooke, W. Simons, C. Rangin, and B. Ambrosius (2006), India and Sunda plates motion and deformation along their boundary in Myanmar determined by GPS, *J. Geophys. Res.*, *111*, B05406, doi:10.1029/2005JB003877.

Thatcher, W., and J. B. Rundle (1979), A model for the earthquake cycle in underthrust zones, *J. Geophys. Res.*, *84*, 5540–5556.

Tse, S. T., and J. R. Rice (1986), Crustal earthquake instability in relationship to the depth variation of frictional slip properties, *J. Geophys. Res.*, *91*, 9452–9472.

R. Bilham, Department of Geological Sciences, University of Colorado, Boulder, CO 80309-0399, USA. (roger.bilham@colorado.edu)

A. R. Lowry, Department of Geology, Utah State University, Logan, UT 84322-4505, USA. (arlowry@cc.usu.edu)

J. Paul and R. Smalley Jr., Centre for Earthquake Research and Information, 3876 Central Ave., Memphis, TN 38152, USA. (jpuchkyl@memphis.edu; rsmalley@memphis.edu)

S. Sen, Society for Andaman and Nicobar Ecology, Port Blair 744101, India. (sumitro.sen@gmail.com)